

Spin-active interfaces and unconventional pairing in half-metal|superconductor junctions

Jacob Linder,¹ Mario Cuoco,^{2,3} and Asle Sudbø¹

¹*Department of Physics, Norwegian University of Science and Technology, N-7491 Trondheim, Norway*

²*CNR-SPIN, I-84084 Fisciano (Salerno), Italy*

³*Dipartimento di Fisica E.R. Caianiello, Università di Salerno, I-84084 Fisciano (Salerno), Italy*

(Dated: Received May 26, 2022)

We study the physical properties of a half-metallic ferromagnet|superconductor (HM|S) bilayer, allowing for an arbitrary bulk pairing symmetry of the superconductor and spin-dependent processes at the interface. In particular, we study how the possibility of unconventional pairing such as p - and d -wave and a spin-active interface influence the (i) conductance spectra, (ii) proximity effect, and (iii) local density of states of such a bilayer. Our calculation is done both analytically and numerically in the ballistic limit, using both a continuum- and lattice-model. It is found that the spin-dependent phase-shifts occurring at the HM|S interface seriously influence all of the aforementioned phenomena. We explain our results in terms of Andreev reflection in the presence of a spin-active interface, allowing for both spin-filtering and spin-mixing processes. We demonstrate how the surface-bound states induced by the anisotropy of the superconducting order parameter at the HM|S interface are highly sensitive to these spin-dependent processes. Our results can be directly tested experimentally using STM-measurements and/or point-contact spectroscopy.

PACS numbers:

I. INTRODUCTION

In recent years, the physics of composite superconductor|ferromagnet systems has been subject to intense investigations. Apart from a wealth of interesting effects to explore from a fundamental physics point of view, it is also hoped that the interplay between the dissipationless current flow in superconductors combined with the spin-polarization in ferromagnets will lead the way to new applications in low-temperature nanotechnology.

The mutual influence of superconducting and ferromagnetic elements in heterostructures has a long history, see Ref.^{1,2} and references therein. While the basic constituent in a superconducting condensate is a spin-singlet Cooper pair in the usual Bardeen-Cooper-Schrieffer³ paradigm, the superconducting correlations are strongly altered when placed in close proximity to a ferromagnetic system, which spontaneously breaks time-reversal symmetry. Whenever translational symmetry or time-reversal symmetry is broken, Cooper pairs with unconventional pairing correlations are formed in general⁴⁻⁶. Such pairing correlations are unconventional in the sense that they differ from the conventional spin-singlet Cooper pairs, and they may exhibit for instance a spin-triplet symmetry or an odd-frequency symmetry. The study of the proximity effect in superconductor|ferromagnet heterostructures has received a lot of attention in recent years (see, *e.g.*, Refs. 7-37).

In the extreme ferromagnetic limit of a half-metal, where the spin-polarization is close to 100%, one would naively expect proximity-induced superconducting correlations to be destroyed due to the large exchange field in the ferromagnet. However, quite surprisingly at the time, Keizer *et al.* found¹⁴ that a supercurrent could flow between two conventional s -wave superconductors separated by a half-metallic layer of considerable size ($\sim \mu\text{m}$). This finding prompted several authors to investigate the underlying physics that permitted the superconducting correlations to survive over a long distance

in a fully polarized ferromagnet^{17,22}.

Prior to the experimental finding in Ref.¹⁴, the concepts of *spin-mixing* and *spin-flip* processes were drawn upon in Ref.¹¹ in order to explain how a supercurrent could be generated and sustained in an s -wave/half-metal/ s -wave junction. The scattering of quasiparticles at the interface may in general be spin-dependent in the presence of magnetic parts of the system, which is the case for a superconductor/ferromagnet junction. This renders the transmission probabilities for spin- \uparrow and spin- \downarrow particles different not only in magnitude, but also through the phases they pick up upon scattering at the interface. This gives rise to a so-called spin-mixing at the interface, which allows the singlet amplitude to be converted into a $S_z = 0$ triplet component, since scattered electrons with opposite spins experience different phase shifts at the interface. As a result, the superconducting correlations become a superposition of both singlet and $S_z = 0$ triplet pairing. It is convenient for later use to briefly recapitulate here how this happens¹¹. Consider a singlet correlation function in the superconductor:

$$|\Psi\rangle = |\uparrow\rangle_k |\downarrow\rangle_{-k} - |\downarrow\rangle_k |\uparrow\rangle_{-k}. \quad (1)$$

Upon scattering at the interface, the spins acquire different phase shifts

$$|\uparrow\rangle_{-k} = e^{i\theta_\uparrow} |\uparrow\rangle_k, \quad |\downarrow\rangle_{-k} = e^{i\theta_\downarrow} |\downarrow\rangle_k. \quad (2)$$

This transforms Eq. (1) into

$$|\Psi\rangle = -\cos(\Delta\theta) \left(|\uparrow\rangle_k |\downarrow\rangle_{-k} - |\downarrow\rangle_k |\uparrow\rangle_{-k} \right) - \sin(\Delta\theta) \left(|\uparrow\rangle_k |\downarrow\rangle_{-k} + |\downarrow\rangle_k |\uparrow\rangle_{-k} \right). \quad (3)$$

Here, $\Delta\theta = \theta_\uparrow - \theta_\downarrow$. The spin-dependent phase-shifts at the interface induce a triplet component which contributes to the total wavefunction $|\Psi\rangle$ as long as $\Delta\theta \neq 0$.

However, it is also necessary to generate an equal-spin pairing $S_z = \pm 1$ components in order to sustain the long-range

triplet correlations. This demands spin-flip scattering processes of the type $|\uparrow\rangle_k \rightarrow |\downarrow\rangle_k$ and $|\downarrow\rangle_k \rightarrow |\uparrow\rangle_k$ close to the interface. Such processes are unavoidably present for instance in the case where there are local inhomogeneities of the magnetic moment near the interface. The combination of spin-mixing and spin-flip processes then explain how the spin-singlet s -wave component of the bulk superconductor may be converted into a long-range spin-triplet component that is able to survive the large exchange field in the half-metallic region.

The above discussion underlines the crucial importance of treating the interface properties correctly, and specifically taking into account the spin-dependent phase-shifts that may occur for the particles participating in the scattering processes³⁹. In addition, the presence of mixed-parity pairing correlations in a S/HM structure should be linked to the spin-active nature of the interface. Previous literature has considered only the proximity effect between conventional s -wave superconductors and half-metallic ferromagnets²². In the present work, our aim is to investigate the interplay between the spin-dependent interface properties and *unconventional* pairing symmetries in the bulk superconductor with regard to the (i) conductance spectra, (ii) proximity effect, and (iii) local density of states of such a bilayer. These quantities are directly accessible in experiments via STM-measurements and/or point-contact spectroscopy. In particular, by allowing for an unconventional pairing symmetry in the superconductor, such as p -wave or

d -wave, we may investigate the interplay between Andreev-bound surface states^{40,41} and half-metallicity.

We organize this work as follows. In Sec. II, we present the theoretical formulation used in this work, namely the Bogoliubov-de Gennes formalism. In Sec. III and IV, we present and discuss our results for the conductance and proximity effect/DOS, respectively. Finally, we give our conclusions in Sec. V. We will use boldface notation for 3-vectors, \dots for 4×4 matrices, and $\underline{\dots}$ for 2×2 matrices.

II. THEORY

In order to calculate the conductance of the S/HM junction, we apply a modified Blonder-Tinkham-Klapwijk (BTK) theory which takes into account both an arbitrary pairing symmetry of the superconductor as well as spin-mixing at the interface. Specifically, we consider the situation as shown in Fig. 1, where the region near the interface is allowed to have misaligned magnetic moments as compared to the bulk of the half-metallic ferromagnet. Our starting point is the BdG-equation

$$\hat{H}\Psi = \epsilon\Psi \quad (4)$$

in the half-metallic and superconducting region. We find that

$$\hat{H} = \begin{pmatrix} H_0 - h_z\Theta(-x) + V_\uparrow\delta(x) & (V_x - iV_y)\delta(x) & 0 & \Delta(\theta)\Theta(x) \\ (V_x + iV_y)\delta(x) & H_0 + h_z\Theta(-x) + V_\downarrow\delta(x) & \zeta\Delta(\theta)\Theta(x) & 0 \\ 0 & \zeta\Delta(\theta)^*\Theta(x) & -H_0 + h_z\Theta(-x) - V_\uparrow\delta(x) & -(V_x + iV_y)\delta(x) \\ \Delta(\theta)^*\Theta(x) & 0 & -(V_x - iV_y)\delta(x) & -H_0 - h_z\Theta(-x) - V_\downarrow\delta(x) \end{pmatrix} \quad (5)$$

upon defining

$$H_0 = -\frac{\nabla^2}{2m} - \mu, \quad V_\sigma = V_0 + \sigma V_z, \quad (6)$$

while $\Theta(x)$ and $\delta(x)$ are the Heaviside step-function and delta-function, respectively. Here, the barrier magnetic moment constitutes a spin-dependent potential, where $V_x = -\rho V_0 \cos \Psi \sin \phi$, $V_y = -\rho V_0 \sin \Psi \sin \phi$, $V_z = -\rho V_0 \cos \phi$. The intrinsic non-magnetic barrier potential is V_0 , while ρ constitutes the effective ratio between the non-magnetic and magnetic barrier, since

$$\rho = |\mathbf{V}|/V_0 \quad (7)$$

where $\mathbf{V} = (V_x, V_y, V_z)$. The parameter ζ accounts for singlet or triplet pairing through $\zeta = -1$ for singlet pairing while $\zeta = 1$ for triplet pairing. In both cases, however, we assume opposite-spin pairing, corresponding to a unitary state in the triplet case. The exchange energy in the half-metallic ferromagnet is modelled through h_z , and we will later take the limit $h_z \rightarrow \mu$, corresponding to a fully polarized ferromagnet.

Solving Eq. (5), we obtain the following wavefunction in the superconducting region:

$$\begin{aligned} \Psi_S(x) = & t_e^\uparrow \left[u(\theta_S), 0, 0, v(\theta_S) e^{-i\gamma_+} \right] e^{iq \cos \theta_S x} \\ & + t_e^\downarrow \left[0, u(\theta_S), \zeta v(\theta_S) e^{-i\gamma_+}, 0 \right] e^{iq \cos \theta_S x} \\ & + t_h^\uparrow \left[0, \zeta v(\pi - \theta_S) e^{i\gamma_-}, u(\pi - \theta_S), 0 \right] e^{-iq \cos \theta_S x} \\ & + t_h^\downarrow \left[v(\pi - \theta_S) e^{i\gamma_-}, 0, 0, u(\pi - \theta_S) \right] e^{-iq \cos \theta_S x}, \end{aligned} \quad (8)$$

while in the ferromagnetic region we have for an incoming spin- \uparrow electron with positive excitation energy ϵ :

$$\begin{aligned} \Psi_{HM}(x) = & \left(e^{ik^\uparrow \cos \theta x} + r_e^\uparrow e^{-ik^\uparrow \cos \theta x} \right) \left[1, 0, 0, 0 \right] \\ & + r_e^\downarrow \left[0, 1, 0, 0 \right] e^{-ik^\downarrow \cos \theta x} \\ & + r_h^\uparrow \left[0, 0, 1, 0 \right] e^{ik^\uparrow \cos \theta_A x} \\ & + r_h^\downarrow \left[0, 0, 0, 1 \right] e^{ik_A^\downarrow \cos \theta_A x}. \end{aligned} \quad (9)$$

In the above equations, $\{t_e^\sigma, t_h^\sigma\}$ denote the transmission coefficients for electron-like and hole-like quasiparticles in the superconductor with spin σ . Note that without any spin-mixing at the interface, one has $t_e^\downarrow = t_h^\uparrow = 0$ in the present case. This is because that an incoming spin- \uparrow from the HM side can only be reflected normally in such a scenario without conversion at the interface. We comment more on this later. Moreover, q denotes the Fermi-level momentum in the S region while θ_S is the propagation angle. The coherence functions are defined in the standard way:

$$\begin{aligned} u(\theta) &= \sqrt{\frac{1}{2} \left(1 + \frac{\sqrt{\epsilon^2 - |\Delta(\theta)|^2}}{\epsilon} \right)}, \\ v(\theta) &= \sqrt{\frac{1}{2} \left(1 - \frac{\sqrt{\epsilon^2 - |\Delta(\theta)|^2}}{\epsilon} \right)} \end{aligned} \quad (10)$$

We have also introduced the phase factors

$$e^{i\gamma_\pm} = \Delta(\theta_\pm)/|\Delta(\theta_\pm)| \text{ with } \theta_+ = \theta, \theta_- = \pi - \theta. \quad (11)$$

In the normal region, we have artificially included scattering-coefficients for spin- \downarrow since our strategy is to do the calculation for a strong ferromagnet, and finally take the half-metallic limit, corresponding to $\{k^\uparrow, k_A^\uparrow\} \rightarrow 0$. In the final expression for the conductance, the contribution from minority spin will be down a factor $|k^\uparrow/k^\downarrow| \rightarrow \infty$ compared to the majority spin contribution, which gives us the correct result in the half-metallic limit. We choose $q = k^\uparrow$, assuming that Fermi-vector mismatch effects simply alter the effective barrier resistance. In this case, $\theta_S = \theta$.

The task at hand is now to calculate the scattering coefficients, which are needed to evaluate the conductance. To do so, we need to incorporate proper boundary conditions. The presence of a magnetic moment in the barrier, which is not necessarily aligned with the magnetization in the bulk HM region, introduces new components in the boundary conditions as compared to the ones that mostly have been used in the literature. Assuming a barrier with a spin-independent potential V_0 and a spin-dependent potential of strength ρV_0 , where the orientation of the magnetic moment is described by two angles $\{\phi, \Psi\}$ as shown in Fig. 1, we may write:

$$\begin{aligned} \partial_x[\Psi_S(x) - \Psi_{HM}(x)]|_{x=0} &= 2mV_0[\hat{1} - \rho \cos\phi(\underline{\tau}_0 \otimes \underline{\sigma}_3) \\ &\quad - \rho \sin\phi \hat{M}(\Psi)]\Psi_{HM}(0), \end{aligned} \quad (12)$$

where we have defined the matrices

$$\hat{M}(\Psi) = \begin{pmatrix} \underline{\Theta}(\Psi) & 0 \\ 0 & \underline{\Theta}^*(\Psi) \end{pmatrix}, \quad \underline{\Theta}(\Psi) = \begin{pmatrix} 0 & e^{-i\Psi} \\ e^{i\Psi} & 0 \end{pmatrix} \quad (13)$$

In addition, continuity of the wavefunction gives $\Psi_{HM}(0) = \Psi_S(0)$. Using these boundary conditions with Eqs. (8) and (9), one obtains the solution for the scattering coefficients. Then, the conductance of the junction is expressed at zero temperature through the dimensionless quantity

$$G(eV) = \int_{-\pi/2}^{\pi/2} d\theta f(\theta) [1 + |r_h^\uparrow(eV)|^2 - |r_e^\uparrow(eV)|^2]. \quad (14)$$

Here, $f(\theta)$ is an angle-dependent factor which models the probability distribution for incoming electrons at an angle θ . Usually, it is chosen to $f(\theta) = \cos\theta$ to favor angles close to normal incidence, but it may also be chosen to exhibit a more discriminating tunneling cone behavior. In all the plots, we will normalize the conductance on its value at voltages much larger than the gap, i.e. $eV \gg \Delta_0$, as is usually done when comparing against experimental data since this regime corresponds to the normal-state conductance, and we choose $f(\theta) = \cos\theta$.

Although an analytical solution for the scattering coefficients is possible in principle, the resulting expressions are somewhat cumbersome, so we omit them here. For a fixed pairing symmetry $\Delta(\theta)$, the interface properties will determine the behavior of the junction conductance. The interface parameters are then the spin-independent barrier strength $Z = 2mV_0/q$, the ratio between the spin-independent and spin-dependent scattering potential ρ , and the orientation of the barrier magnetic moment determined by ϕ and Ψ . All of these quantities are dimensionless.

In what follows, we will fix the barrier strength at $Z = 3$ corresponding to a weakly transparent interface, since this should correspond to a realistic experimental situation. All the interesting physics then lies in the parameters $\{\rho, \phi, \Psi\}$. In the experimental work so far, strong sample-to-sample variations are seen in the results for the conductance and the critical current of S/HM heterostructures. As pointed out in Ref.²², this is an indication that the spin-properties of the interface vary greatly between different samples, suggesting that the quantities $\{\rho, \phi, \Psi\}$ are very hard to control experimentally. The purpose of this paper is to obtain a fuller picture of how the spin-active properties of the interface influence the conductance spectra in order to gain a clearer understanding of the characteristic features seen in the experimental data.

III. RESULTS: CONDUCTANCE

Before we proceed to a dissemination of our results, let us establish contact between the terminology and notation used in previous literature regarding proximity structures of superconductors and half-metallic ferromagnets. In our notation, spin-mixing corresponds to the case of a finite ρ , but with $\phi = 0$. In this case, the effective potential felt by spin- \uparrow and spin- \downarrow electrons scattered at the interface is different, and they pick up different phases along their scattering trajectories. Note that the spin-dependent potential also gives rise to, in general, a magnetoresistance effect known as spin-filtering since the transmission amplitudes for opposite spins are not the same. Spin-flip scattering, however, requires a misalignment between the barrier magnetic moment and the bulk magnetization in the half-metallic ferromagnet. In our notation, it is then necessary to have $\rho \neq 0$ and also $\phi \neq 0$. Only then will the scattering amplitudes t_e^\downarrow and t_h^\uparrow be non-zero in general, as commented on earlier. From Fig. 1, it is clear that it suffices to vary only ϕ in order to obtain both spin-mixing and spin-flip processes. To reduce the number of free parameters and still grasp the key physics, we therefore set $\Psi = \pi/2$ in what follows. In this way, the barrier magnetic moment lies

in the $y-z$ plane. Spin-mixing is then obtained for $\rho \neq 0$ and $\phi = 0$, while spin-mixing *and* spin-flip processes are obtained for $\rho \neq 0$ and $\phi \neq 0$.

So far in the literature, the interplay between unconventional bulk superconductivity and half-metals has not been studied yet. We will therefore consider several bulk pairing symmetries in the superconducting region, including p - and d -wave pairing.

A. s -wave pairing

For s -wave pairing, we choose $\Delta(\theta) = \Delta_0$. Consider first the situation of pure spin-mixing, corresponding to $\rho \neq 0$, while $\phi = 0$. This is shown in the first row of Fig. 2 (left panel), where it is seen that the sharp coherence peak at the gap is replaced with broadened features upon increasing ρ . This is in agreement with Fig. 2 of Ref.³⁸ for high values of their parameter R , which corresponds roughly to our Z . Note that the subgap conductance is exactly zero, regardless of the value of ρ . The reason for this is that the usual Andreev-reflection where the hole has opposite spin of the incoming electron is not possible in the present case of a half-metal, unless spin-flip processes are allowed at the interface. Interestingly, Andreev-reflection is therefore absent in the system regardless, in fact, of the value of Z unless there is a magnetically inhomogeneous region near the interface. We will discuss this on a microscopic level in much more detail in Sec. III D.

To illustrate how spin-flip processes affect the conductance, we show in Fig. 2 (right panel) the case of $\rho = 0.5$ for several values of ϕ . As seen, once ϕ becomes non-zero, the sub-

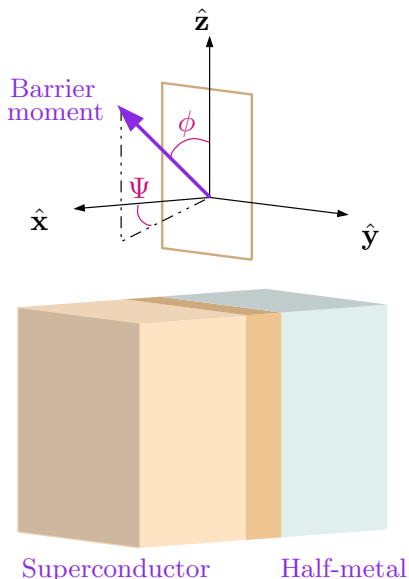


FIG. 1: (Color online) The superconductor/half-metallic ferromagnet bilayer studied in this paper. The barrier magnetic moment may in general be misaligned to the bulk magnetization in the ferromagnet, which is assumed to be directed along \hat{z} . The presence of a barrier magnetic moment may lead to both spin-split and spin-flip processes at the interface.

gap conductance becomes finite. A large peak very close to $eV = \Delta_0$ evolves with increasing ϕ . However, the zero-bias conductance remains suppressed regardless of the orientation of the barrier moment. In Ref.⁴³, the conductance was experimentally measured for a Pb/La_{0.7}Sr_{0.3}MnO₃ point contact setup, where the authors found strong sample-to-sample variations. Some of the samples showed clear zero-bias conductance peaks, which is usually a signature of odd-frequency correlations or zero-energy Andreev-bound states. Other samples displayed a clear minigap structure similar to our finding in Fig. 2 for the s -wave case. The strong zero-bias peak observed in the samples led the authors of Ref.⁴³ to speculate that an even-frequency p -wave bulk state was induced in half-metallic La_{0.7}Sr_{0.3}MnO₃ by means of the proximity to superconducting Pb, thus rendering the Pb/La_{0.7}Sr_{0.3}MnO₃ junction into an S/S junction. Another observation in Ref.⁴³ that supported this idea was a spectacular drop of the contact's resistance with the onset of the Pb superconductivity.

B. p -wave pairing

For p -wave pairing, we will consider a gap of the form $\Delta(\theta) = \Delta_0 e^{i\theta}$. This is known as chiral p -wave or $p_x + ip_y$ -wave pairing, and is believed to be realized in Sr₂RuO₄. The gap supports Andreev-bound zero-energy states at normal incidence of incoming quasiparticles, $\theta = 0$, where it satisfies the appropriate symmetry condition $\Delta(\theta) = -\Delta(\pi - \theta)$. The situation changes, however, in the present case where the non-superconducting region is half-metallic. Let us first consider the case of pure spin-mixing ($\phi = 0$) in the second row of Fig. 2 (left panel). As seen, the subgap conductance is still zero, since the gap magnitude $|\Delta(\theta)|$ is isotropic and thus prevents direct quasiparticle tunnelling into any nodes of the gap. Also, the usual zero-energy Andreev-bound states do not take part in the scattering processes since there is no possibility for Andreev-reflection of a spin- \downarrow hole in the half-metal.

The situation changes drastically once we introduce magnetic inhomogeneities at the interface (right panel), corresponding to $\phi \neq 0$. The subgap conductance, in particular the zero-bias conductance, is greatly enhanced upon increasing ϕ . The reason is that although no spin- \downarrow holes are available in the half-metal, the presence of spin-flip scattering when $\phi \neq 0$ allows for Andreev reflection with spin- \uparrow holes. The presence of Andreev reflection of majority spin holes is the reason for the enhancement of the conductance.

C. d -wave pairing

For d -wave pairing, we choose $\Delta(\theta) = \Delta_0 \cos(2\theta - 2\alpha)$. For $\alpha = 0$, there are no Andreev-bound states, while for $\alpha = \pi/4$ the order parameter supports the formation of Andreev-bound states in a N| d -wave junction. Consider first the case with only spin-mixing at the interface, i.e. $\phi = 0$. The existence of nodes in the gap renders the subgap conductance non-zero for both crystallographic orientations $\alpha = 0$ and $\alpha = \pi/4$. The effect of increasing ρ is opposite for the two orientations. For

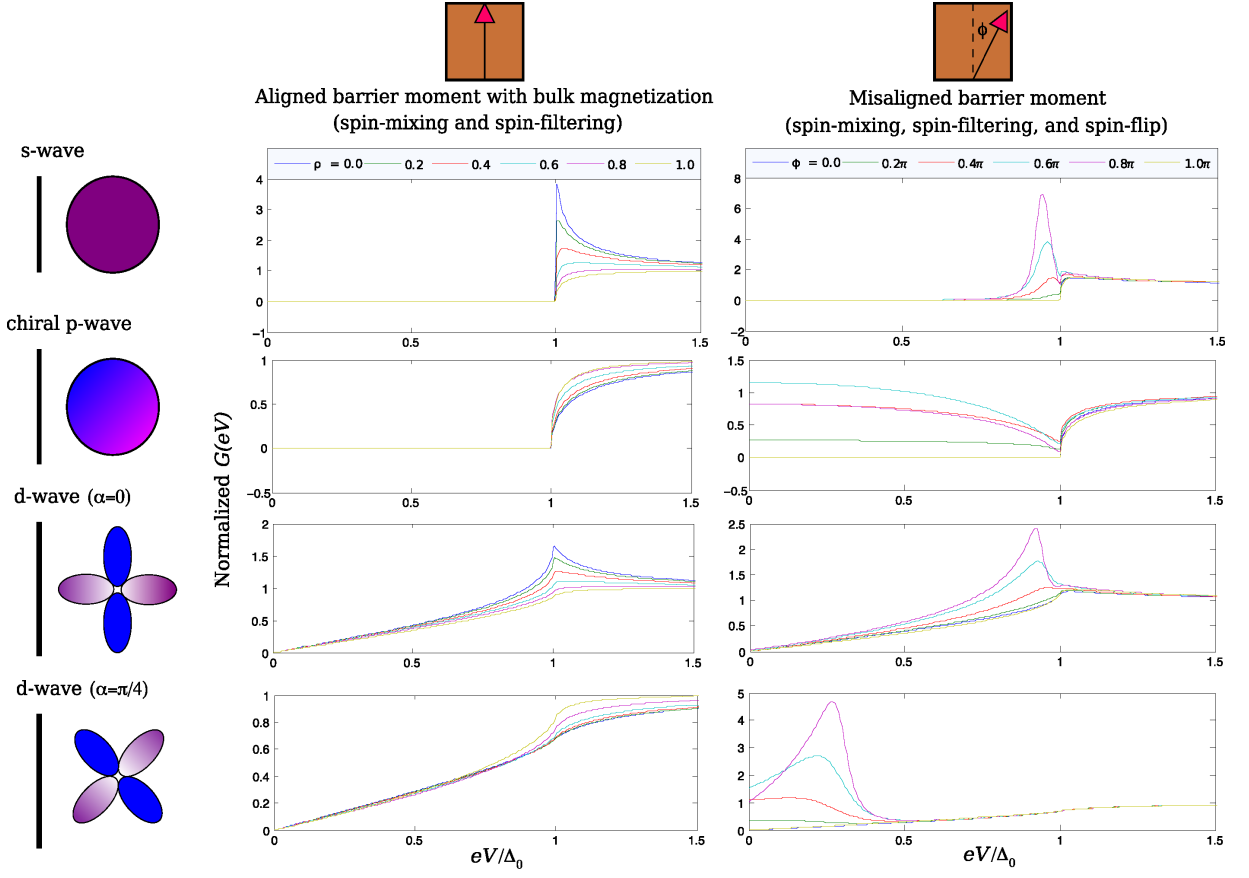


FIG. 2: (Color online) Plot of the normalized conductance $G(eV)$ for a s -wave, chiral p -wave, $d_{x^2-y^2}$ -wave, and d_{xy} -wave symmetry in the rows ranging from top to bottom. In the left panels, we consider the case of pure spin-mixing for several values of ρ with $\phi = 0$. In the right panels, we consider additionally spin-flip processes induced by a misaligned barrier moment at the interface for several values of ϕ with $\rho = 0.5$.

$\alpha = 0$, the conductance evolves from the typical d -wave bulk density of states profile at $\rho = 0$ to exhibit broader features at $\rho \simeq 1$. For $\alpha = \pi/4$ the conductance evolves from broad features at $\rho = 0$ to a typical d -wave bulk density of states at $\rho \simeq 1$.

Introducing spin-flip processes at the interface by allowing $\phi \neq 0$, the distinction between the two crystallographic orientations becomes clear. For $\alpha = 0$, the conductance is similar to the bulk density of states, while for $\alpha = \pi/4$ the zero-bias conductance is strongly enhanced upon increasing ϕ . For the same reason as described in the chiral p -wave case, this enhancement is a result of the spin-flip induced Andreev reflection of spin- \uparrow holes made possible by $\phi \neq 0$. Interestingly, a large peak evolves at an energy inside the gap similarly to the s -wave case. One may thus ask whether the presence of a sub-gap peak in the conductance is indicative of surface bound-states induced by the spin-active interface. We shall discuss this question in more detail in the following section.

D. Analytical expressions and bound-states

In order to understand further the above results, it is instructive to consider analytically the expression for the scattering coefficients. In particular, we focus on the Andreev reflection probability r_h^\uparrow which only exists for \uparrow -spin in the HM region. We find that the following general expression:

$$r_h^\uparrow = -4\rho ZR^{-1} \sin\phi \cos^2\theta e^{i\beta - i\gamma} \left[iZ(1 + \rho \cos\phi)(1 + \zeta) \times (e^{-i\Delta\gamma} - e^{2i\beta}) - \cos\theta(1 - \zeta)(e^{-i\Delta\gamma} + e^{2i\beta}) \right], \quad (15)$$

where we have defined $e^{i\beta} = u(\theta)/v(\theta)$ and

$$R = Z^4(1 - \rho^2)^2(e^{2i\beta} - e^{-i\Delta\gamma})^2 + 4\cos^4\theta e^{4i\beta} + Z^2\cos^2\theta \times \left[e^{-2i\Delta\gamma}(1 - \rho \cos\phi)^2 + e^{2i\beta - i\Delta\gamma}[4\rho(\rho - \cos\phi) - (1 - \cos^2\phi)] + e^{4i\beta}(6\rho \cos\phi + 4\rho^2 + \rho^2 \cos^2\phi + 5) \right]. \quad (16)$$

Note that r_h^\uparrow vanishes when either ϕ , ρ , or Z are equal to zero. This is physically reasonable, since the interface be-

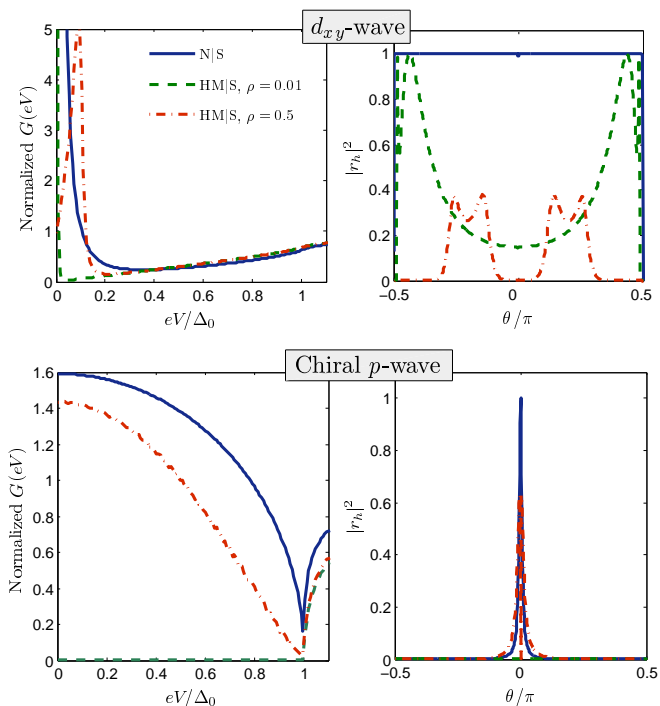


FIG. 3: (Color online) Comparison of the conductance spectra for N|S and HM|S junctions with a d_{xy} -wave superconductor in the top row and a chiral p -wave superconductor in the bottom row. In the half-metallic case, we consider a spin-active interface with a misorientation angle $\phi = 0.5$. The ratio between the magnetic and non-magnetic part of the barrier potential is denoted ρ . In all cases, the strong tunneling limit $Z = 10$ is considered. The Andreev reflection probability in the right panels is calculated at the peak energy in the d_{xy} -wave case while it is calculated at $\epsilon = 0$ in the chiral p -wave case.

comes spin-inactive in all those cases. Hence, there are no spin-flip processes which can mediate Andreev reflection r_h^\uparrow . Consider now the triplet pairing case $\zeta = 1$. In a normal metal|chiral p -wave superconductor junction, it is well-known that the bound-state energies at the interface have a dispersion $\epsilon \sim \Delta_0 \sin \theta$. More specifically, the bound-state condition is given by

$$2\beta = -\Delta\gamma = \pi - 2\theta. \quad (17)$$

Interestingly, the Andreev-reflection coefficient Eq. (15) vanishes completely for precisely these energies, regardless of the other parameters in the system. This is then opposite to the N|chiral p -wave case where the Andreev reflection coefficient is unity at the bound-state energies.

In the previous section, we pointed to the possibility that the emergence of strong peaks in the subgap conductance seen in both the s - and d_{xy} -wave cases is a signature of surface bound-states. This would be similar to the zero-bias conductance peak in N| d_{xy} -wave junctions originating from the existence of zero-energy surface states. It should be noted that an enhancement of the conductance above its normal-state value is in general not sufficient to prove the existence of surface bound-states. To see this, consider *e.g.* a N| s -wave junction

with a good interface contact ($Z \leq 1$), where Andreev reflection occurs with a high probability even without any interface bound-states. To clarify whether an enhancement of the conductance (such as a resonant peak-structure) truly pertains to surface bound-states, one has to consider the tunneling limit of a strong barrier potential, or equivalently a low interface transparency. If the conductance is still enhanced compared to its normal-state value due to the presence of Andreev reflection, it *could* be a signature of resonant tunneling into a surface-state. We now compare the behavior of the Andreev reflection probability in the half-metallic limit with the corresponding non-magnetic case in order to acquire information about the origin of the conductance peak. In the top row of Fig. 3, we plot the conductance of a N| d_{xy} -wave junction (without a spin-active interface) and a HM| d_{xy} -wave junction as well as the respective Andreev reflection probabilities at the peak energies. The Andreev reflection probability $|r_h|^2$ is given as a function of the angle of incidence θ . For all plots, we have set $Z = 10$, corresponding to strong tunneling limit.

In the normal metal case, the usual ZBCP is recovered and the Andreev reflection probability is unity for all angles of incidence. Thus, charge is transmitted into the superconductor as a Cooper pair via the resonant zero-energy states. Turning to the HM case, we wish to distinguish between the two cases of a weak and strong magnetic moment of the barrier. For $\rho = 0.01$, it is seen that the ZBCP remains, while for $\rho = 0.5$ the ZBCP is shifted to a finite bias voltage. In the latter case, similar behavior was also reported for a N| d_{xy} -wave junction with a spin-active interface in Ref.⁵². In our case, it is necessary to have a non-zero misalignment angle ϕ between the barrier moment and the bulk magnetization in order to generate Andreev reflection at all, contrary to the scenario of Ref.⁵². However, the Andreev reflection coefficients shown for the d_{xy} -wave case in Fig. 3 indicate that the peaks cannot be ascribed to resonant energy states that are available at all angles of incidence. In fact, the probability for Andreev reflection never reaches unity when $\rho = 0.5$. Still, $|r_h^\uparrow|^2$ is substantial in magnitude even though we are considering the tunneling limit. It therefore appears that surface-states are induced close to the interface which enable transmission processes in spite of the large barrier potential, although they are not resonant in the sense that transmission into them occurs with a probability of unity.

Turning now to the chiral p -wave case in the lower row of Fig. 3, we see that the subgap conductance remains completely suppressed when ρ is small. This contrasts with the d_{xy} -wave case. We next increase the magnitude of the magnetic part of the barrier compared to the non-magnetic part further, *i.e.* we increase ρ . It is now seen that the subgap conductance then becomes comparable to the N|chiral p -wave case. Note that both spin species see an effective barrier potential in the tunnelling limit even for $\rho = 0.5$ due to the large value of Z . Therefore, the large enhancement of the subgap conductance must stem from surface-induced states which decay inside the bulk. In the following section, we will employ a self-consistent Bogoliubov-de Gennes framework to numerically investigate whether the local DOS near the interface truly features such surface-bound states or not.

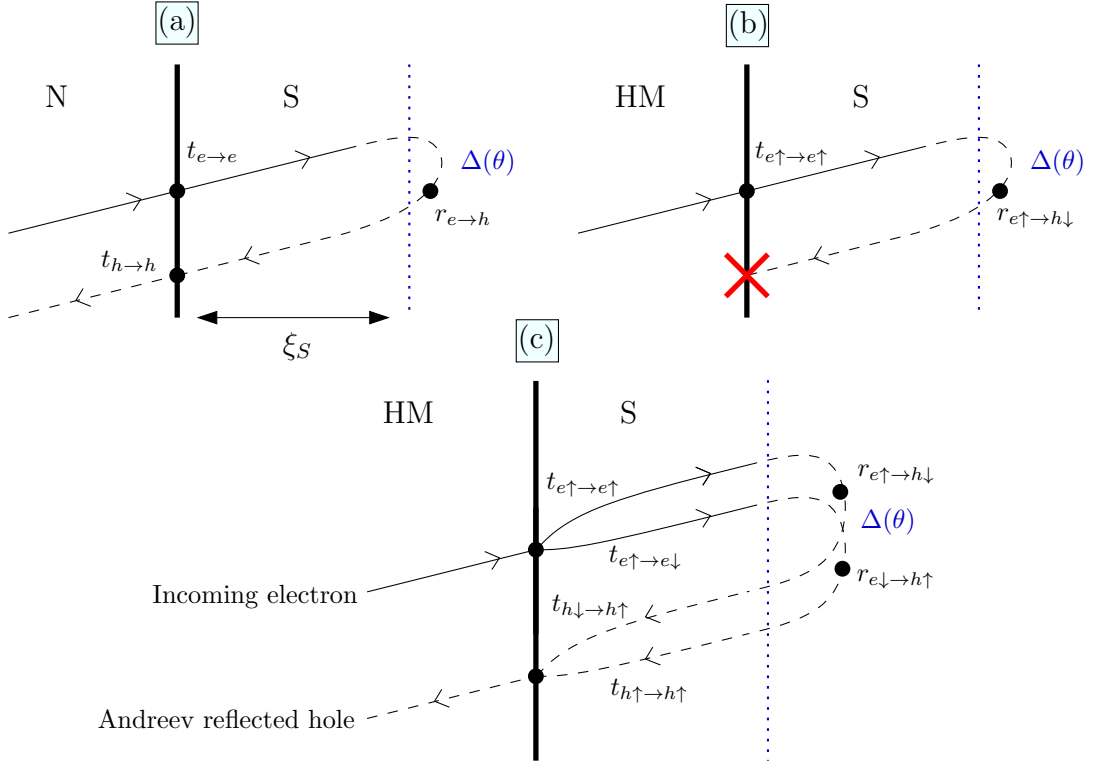


FIG. 4: (Color online) Andreev reflection scattering to first order for three cases: (a) N|S junction without spin-active interface, (b) HM|S junction without spin-active interface, (c) HM|S junction with spin-active interface. The incoming electron-like quasiparticle penetrates the superconducting region a distance ξ_S before being backscattered as a hole by the superconducting gap.

To understand how the spin-active interface influences Andreev reflection and midgap bound states on a microscopic level, it is useful to again compare the N|S case with the HM|S case. The Andreev reflection process to first order is shown in Fig. 4. Higher order processes may be generalized from the first order process along the lines of Ref.⁵³. From Fig. 4, the general recipe for Andreev reflection is seen to be a transmission of an electron-like quasiparticle into the superconductor, which penetrates about a coherence length ξ_S before it is scattered back as a hole by the gap $\Delta(\theta)$. Finally, the hole-like quasiparticle is transmitted to the non-superconducting region. In Fig. 4(a), the Andreev reflection coefficient to first order is thus seen to be $r_h^{(1)} = t_{h \rightarrow h} r_{e \rightarrow h} t_{e \rightarrow e}$, and the contribution from higher order processes is built along the same lines. We have omitted spin indices since the spin for each process is uniquely defined: transmission preserves spin while Andreev reflection flips spin. In Fig. 4(b), we consider a HM|S junction without a spin-flip processes at the interface, corresponding to $\phi = 0$. As seen, Andreev reflection is rendered impossible since the spin- \downarrow hole backscattered by the gap $\Delta(\theta)$ cannot be transmitted into the half-metallic region due to the vanishing DOS for minority spin there. We restrict our attention to opposite spin-pairing superconductors only, such as s -wave, chiral p -wave ($S_z = 0$), and d -wave. For an equal spin-pairing superconductor, Andreev reflection is obviously possible even without any spin-flip processes at the interface. In Fig. 4(c), we consider a HM|S junction with spin-flip processes at the

interface. As mentioned previously, Andreev reflection is now possible even for a backscattered minority spin hole due to the spin-flip probability at the interface.

The microscopic picture shown in Fig. 4 also allows us to understand how the midgap bound states are influenced by the spin-active interface. To do so, we first briefly recapitulate the results of Ref.⁵³ for the N|S case without spin-active processes. Focusing on $\varepsilon = 0$ where the retroreflection property holds in the S region, one can calculate the total probability for Andreev reflection obtained by summing all orders of scattering diagrams such as the ones shown in Fig. 4. In doing so, the total probability is proportional to $|\sum_{n=0}^{\infty} |r|^{2n} [-e^{i(\gamma_- - \gamma_+)}]^n|^2$, where γ_{\pm} represents the phase contribution from the internal phase of the superconducting order parameter while $|r| = |r_{e \rightarrow e}| = |r_{h \rightarrow h}|$. For a d_{xy} -wave superconductor where $e^{i(\gamma_- - \gamma_+)} = -1$, it is seen that all orders sum in a coherent way and the total Andreev reflection probability can be shown to equal unity. In the present case, the phases picked up by the scattered particles are longer spin-degenerate. In particular, we see from Fig. 4(c) that the probability for Andreev reflection to first order is equal to

$$r_h^{(1)} = t_{e \uparrow \rightarrow e \uparrow} r_{e \uparrow \rightarrow h \downarrow} t_{h \downarrow \rightarrow h \uparrow} + t_{e \uparrow \rightarrow e \downarrow} r_{e \downarrow \rightarrow h \uparrow} t_{h \uparrow \rightarrow h \uparrow}. \quad (18)$$

The crucial point is now that, whereas the branch-converting reflection coefficients $r_{e \rightarrow h}$ have spin-independent scalar phases without a spin-active interface, they are spin-dependent otherwise. In the former case, one has $r_{e \sigma \rightarrow h, -\sigma} \sim$

$e^{-i\gamma(\theta)+i\vartheta}$ and $r_{h\sigma \rightarrow e,-\sigma} \sim e^{i\gamma(\theta)-i\vartheta}$ with $\sigma = \uparrow, \downarrow$. When summing the Andreev reflection processes to all orders, one obtains products of $r_{e\sigma \rightarrow h,-\sigma}$ and $r_{h\sigma \rightarrow e,-\sigma}$ which effectively gives a phase-factor $e^{i(\gamma-\gamma_+)}$ while the other scalar phases cancel each other. When the interface is spin-active, the scalar phases ϑ become spin-dependent, and one effectively gets an additional contribution $\Delta\vartheta_\sigma = \vartheta_\sigma - \vartheta_{-\sigma}$ in the phase of the effective Andreev reflection coefficient. For this reason, the summation over all orders n is altered and the resonant states at *e.g.* $\varepsilon = 0$ in the d_{xy} -wave case are shifted. The spin-dependent phase-shifts ϑ_σ depend on both ρ and ϕ and are the reason for why the conductance is qualitatively altered in the presence of a spin-active interface as shown in both Fig. 2 and Fig. 3.

IV. PROXIMITY EFFECT AND LOCAL DENSITY OF STATES: A LATTICE STUDY

In this section, within a self-consistent scheme of computation, we investigate the proximity effect and its influence on both the superconducting order parameter and the local density of states in the HM|S bilayer for a model system as described in the Fig. 5. The analysis is based on the case of a junction configuration with the barrier aligned along the y direction in the xy plane. The pairing amplitudes are expressed in terms of the components along the x and y axes of the square lattice. In particular, within such configuration, due to the symmetry properties of the examined order parameters, we do expect that Andreev bound states are effective only for the chiral p -wave paired state (for the analysis on the lattice we do not consider the case of d_{xy} symmetry of the superconducting order parameter). The formalism to be used when calculating the order parameter profile and the density of states is based on a lattice BdG-approach similar to that adopted in Ref.⁴² but extended to the case of a spin active interface. The total Hamiltonian H of the system may be written as

$$H = H_F + H_S + H_T + H_I, \quad (19)$$

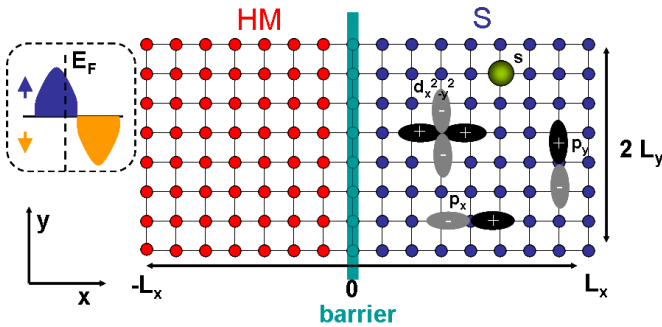


FIG. 5: (Color online) Schematic description of the lattice geometry for the HM|S bilayer junction indicating the reference axis system, the notation for the size ($2L_x \times 2L_y$), the position of the barrier ($x = 0$), the sketch of the pairing configurations (d-wave, p-wave and local s-wave), respectively. On the left side, we show a sketch of the density of states for the half-metal.

where H_F and H_S accounts for the ferromagnetic and superconducting layers, while H_T and H_I describe the tunnelling processes and the scattering potential at the interface region. We have

$$H_I = -\sum_{\langle \mathbf{i}, \mathbf{j} \rangle, \sigma} t_{l\sigma} (c_{i\sigma}^\dagger c_{j\sigma} + \text{h.c.}) + \sum_{\mathbf{i}} U_A n_{i\uparrow} n_{i\downarrow} + \sum_{\langle \mathbf{i}, \mathbf{j} \rangle} V_A (n_{i\uparrow} n_{j\downarrow} + n_{i\downarrow} n_{j\uparrow}) - \mu \sum_{\mathbf{i}, \sigma} n_{i\sigma} - h_A \sum_{\mathbf{i}, \sigma} (n_{i\uparrow} - n_{i\downarrow}), \quad l = F, S, \quad (20)$$

where $\langle \mathbf{i}, \mathbf{j} \rangle$ denotes nearest-neighbor sites, $\{c_{i\sigma}^\dagger, c_{i\sigma}\}$ are creation and annihilation operators of an electron with spin σ on site $\mathbf{i} = (i_x, i_y)$, while $n_{i\sigma}$ is the number operator. We take the exchange field to be non-zero only on the ferromagnetic side, where we let $h_F \rightarrow \mu$ in correspondence with our assumption of a half-metallic limit. The hopping amplitudes are chosen such that $t_{F\uparrow} = t_{F\downarrow} = t_{S\uparrow} = t_{S\downarrow} = t$. Above, μ is the chemical potential, while U_l and V_l denote on-site and nearest-neighbor interaction on side l .

The two layers communicate by means of the tunneling Hamiltonian term, which reads

$$H_T = -t_T \sum_{\langle \mathbf{i}, \mathbf{j} \rangle, \sigma} (c_{i\sigma}^\dagger c_{j\sigma} + \text{h.c.}), \quad (21)$$

where the sites $\langle \mathbf{i}, \mathbf{j} \rangle$ are located at the surface of the F and S layer. Finally, the scattering potential at the interface is modelled through the term

$$H_I = \sum_{i\alpha\beta} c_{i\alpha}^\dagger [V_0 \underline{1} + \mathbf{V}_M \cdot \underline{\sigma}]_{\alpha\beta} c_{i\beta}, \quad (22)$$

where $\{\alpha, \beta\}$ are spin-indices, while \mathbf{i} denotes a lattice site on the surface of the F or S layer (for convenience the interface has been placed at the site $x = 0$ as indicated in Fig. 5). Here, V_0 is a spin-independent scattering potential, roughly corresponding to the parameter Z introduced previously, while \mathbf{V}_M is a spin-dependent scattering potential which gives rise to spin-mixing and spin-flip processes. The Pauli-vector matrix is given as $\underline{\sigma} = (\underline{\sigma}_x, \underline{\sigma}_y, \underline{\sigma}_z)$ and $\underline{1}$ is the 2×2 identity matrix. To facilitate comparison with the notation and parameters used when calculating the conductance, we similarly define

$$\mathbf{V}_M = -\rho V_0 (\cos \Psi \sin \phi, \sin \Psi \sin \phi, \cos \phi), \quad (23)$$

such that ρ denotes the relative weight of the spin-independent and spin-dependent potential while $\{\phi, \Psi\}$ provides the direction of the magnetic moment at the interface. We analyze the effects of the spin-active barrier on the amplitude and the phase of the superconducting order parameter by solving the BdG equations on the lattice within the extended Hubbard model introduced above. The calculation is performed for the case of a planar bilayer junction of dimension $2L_x \times 2L_y$. We have considered lattice sizes of $L_x = L_y = 40, 50, 60$ (lattice constant is the unit of length). The results obtained do not show qualitative nor significant quantitative changes for these values of L_x, L_y . The case studied here corresponds to superconducting and magnetic coherence length of the order of $\xi_S \simeq 7$ and $\xi_{HM} \simeq 1$. Hence, size effects can be considered negligible for the systems we consider. Concerning the ratio

ξ_S/ξ_{HM} , other computations have been performed at different values of the pairing strength V , thus varying ξ_S . These cases do not show qualitative changes in the results. In this framework, the modification of the coherence length is limited by two conditions: i) the requirement of stable superconducting solutions in the phase diagram for the order parameters in the desired symmetry depends on the pair coupling, and ii) the computational demand is related to the size of the matrix Hamiltonian. Hereafter, the discussion will focus on the case $L_x=40$. From Eq. 20 and the BdG formalism already described in Ref.⁴², but extended to the case of a spin active barrier, we compute the spatial variation of the superconducting order parameter for different pairing symmetry and as a function of the barrier parameters. Due to the presence of a spin active barrier one has to introduce a four component Bogoliubov basis on each atomic site to take into account both particle-hole spin flip processes as well as the pairing channel of particle-hole resonance. This introduces an extra factor in the computational complexity. In particular, among the various results obtained, the focus is on the modification, due to the split exchange and the spin flip coupling, of the superconducting order parameter evaluated at the HM—S interface versus (ϕ, V_M, V_0) . In doing that, we have to properly choose the interaction strength both in the magnetic as well as in the superconducting subsystem of the junction in order to get the desired microscopic quantum states. To this end, the effective exchange amplitude in the ferromagnetic region is taken as $h_F = 4.0t$ to have a half-metallic behavior and a profile for the z-component of the magnetization with zero spin minority carriers. Furthermore, to get an *s*-wave, *d*-wave and a chiral *p*-wave symmetry within the superconducting region, three different sets of attractive pairing amplitudes and chemical potentials have to be considered⁴². For the onsite

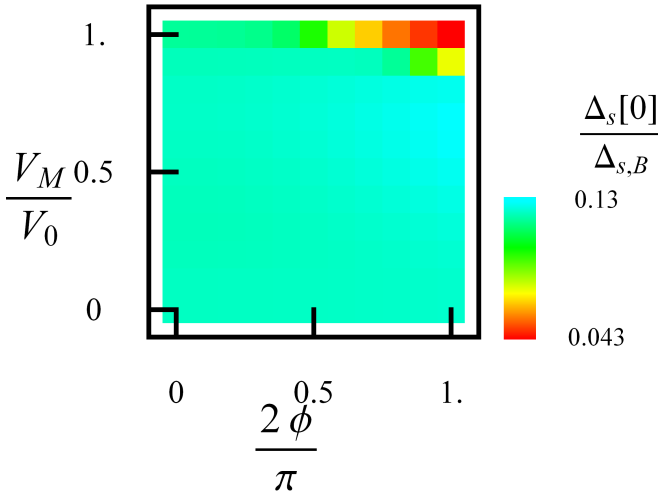


FIG. 6: (Color online) Color map of the *s*-wave on-site pairing amplitude at the interface $\Delta_S[0]$ with respect to the bulk value $\Delta_{S,B}$ as a function of the misalignment angle ϕ and the magnetic barrier strength V_M . The non magnetic scattering potential has an amplitude $V_0 = 2t$.

s-wave, we assume a value of the chemical potential equal to $\mu = -0.2t$, with $U_F = 0, V_F = 0$ for the F side and $U_S = -1.5t, V_S = 0$ for the S side. For the chiral *p*-wave, we choose the value $\mu = -1.6t$, with $U_F = 0, V_F = 0$ within the F side and $U_S = 0, V_S = -2.5t$ for the S side. For the *d*-wave, we choose $\mu = -0.2t$, with $U_F = 0, V_F = 0$ within the F side and $U_S = 0, V_S = -2.5t$ in the S side.

Furthermore, the tunnelling matrix element is kept fixed and chosen equal to $t_T = t$.

The interaction terms in H_F and H_S are decoupled by means of a standard Hartree-Fock approximation such that the magnetic and pairing channels originate from the on-site and the intersite interactions, respectively:

$$\begin{aligned} U_F n_{i\uparrow} n_{i\downarrow} &\simeq U_F [\langle n_{i\downarrow} \rangle n_{i\uparrow} + \langle n_{i\uparrow} \rangle n_{i\downarrow} - \langle n_{i\uparrow} \rangle \langle n_{i\downarrow} \rangle] \\ V_S n_{i\uparrow} n_{j\downarrow} &\simeq V_S [\Delta_{ij} c_{j\downarrow}^\dagger c_{i\uparrow}^\dagger + \Delta_{ij}^* c_{i\uparrow} c_{j\downarrow} - |\Delta_{ij}|^2] \\ U_S n_{i\uparrow} n_{i\downarrow} &\simeq U_S [\Delta_i c_{i\downarrow}^\dagger c_{i\uparrow}^\dagger + \Delta_i^* c_{i\uparrow} c_{i\downarrow} - |\Delta_i|^2] \end{aligned}$$

Here, we have introduced the on-site $\Delta_i = \langle c_{i\uparrow}^\dagger c_{i\downarrow} \rangle$ and the bond pairing amplitude on a bond $\Delta_{ij} = \langle c_{i\uparrow}^\dagger c_{j\downarrow} \rangle$, with the average $\langle K \rangle$ yielding the expectation value of the operator K over the ground state. Moreover, the on site z-component $m_{zi} = \frac{1}{2}(\langle n_{i\uparrow} \rangle - \langle n_{i\downarrow} \rangle)$ and the (x,y)-components of the magnetization $m_{xi} = \frac{1}{2}(\langle c_{i\uparrow}^\dagger c_{i\downarrow} + h.c. \rangle), m_{yi} = \frac{i}{2}(\langle c_{i\uparrow}^\dagger c_{i\downarrow} - h.c. \rangle)$ are iteratively determined up to the required accuracy to get the spatial dependence of the vector spin polarization. From the pairing amplitudes, it is possible to construct the superconducting profiles for the different symmetries (*d*- and *p*-wave) in the singlet (S) and triplet (T) channel in terms of components of the z-projected axial spin operator. They are defined as

$$\begin{aligned} \Delta_d(\mathbf{i}) &= (\Delta_{i,i+\hat{x}}^{(S)} + \Delta_{i,i-\hat{x}}^{(S)} - \Delta_{i,i+\hat{y}}^{(S)} - \Delta_{i,i-\hat{y}}^{(S)})/4 \\ \Delta_{p_x}(\mathbf{i}) &= (\Delta_{i,i+\hat{x}}^{(T)} - \Delta_{i,i-\hat{x}}^{(T)})/2 \\ \Delta_{p_y}(\mathbf{i}) &= (\Delta_{i,i+\hat{y}}^{(T)} - \Delta_{i,i-\hat{y}}^{(T)})/2 \end{aligned}$$

for $d_{x^2-y^2}$, p_x and p_y -wave, respectively. Here one has to introduce the singlet and triplet pairing amplitudes on a bond, given by

$$\begin{aligned} \Delta_{ij}^S &= (\Delta_{ij} + \Delta_{ji})/2 \\ \Delta_{ij}^T &= (\Delta_{ij} - \Delta_{ji})/2 \end{aligned}$$

We adopt open (periodic) boundary conditions for the direction x perpendicular (y parallel) to the interface, taking the Fourier transform due to the translational invariance along the y direction of the relevant physical quantities.

In order to understand the role of the spin active barrier in tuning amplitude and phase of the different symmetry order parameters we have investigated their evolution in terms of the barrier parameters at zero temperature. The angle ϕ tunes the direction of the barrier spin moment from parallel to the z -quantization axis at $\phi = 0$ to being parallel to the x -direction for $\phi = \pi/2$. Different values of Ψ do not change the results due to the $x - y$ symmetry in the spin space. Thus, it suffices

to consider the case $\Psi = 0$. Furthermore, we have chosen one representative case for the regime of nonmagnetic barrier strength that corresponds to a situation of reduced electron density at the interface compared to the electron distribution in the HM and S sides. In this respect, the way of introducing a scattering potential at the interface may lead to extra effects if compared to the delta potential considered in the BTK for-

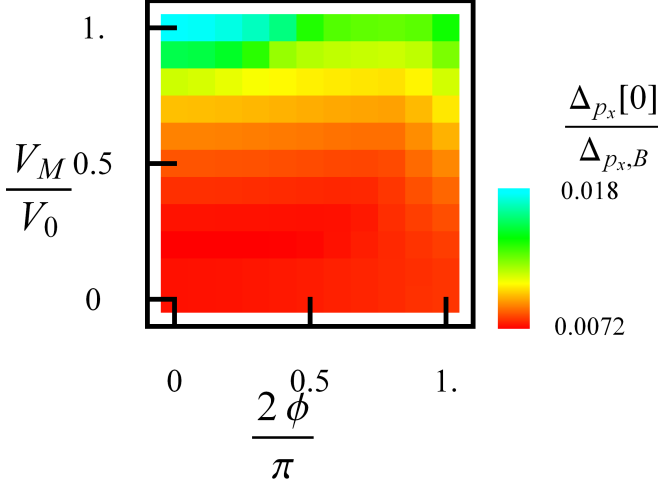


FIG. 7: (Color online) Color map of the real part of the p_x component of the pairing amplitude evaluated at the interface $\Delta_{p_x}[0]$ with respect to the bulk value $\Delta_{p_x,B}$ as a function of the scaled misalignment angle $2\phi/\pi$ and the ratio of the magnetic barrier strength with respect to the nonmagnetic one, V_M/V_0 . The non magnetic scattering potential has a given amplitude of $V_0 = 2t$.

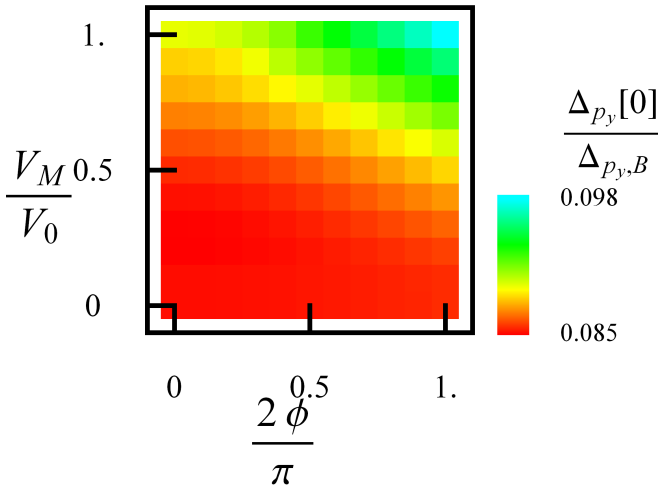


FIG. 8: ((Color online) Color map of the imaginary part of the p_y component for the pairing amplitude evaluated at the interface $\Delta_{p_y}[0]$ with respect to the bulk value $\Delta_{p_y,B}$ as a function of the scaled misalignment angle $2\phi/\pi$ and the ratio of the magnetic barrier strength with respect to the nonmagnetic one, V_M/V_0 . The non magnetic scattering potential has an amplitude $V_0 = 2t$.

malism, since the amplitude of the non magnetic potential determines the average electron occupation at the barrier site as well as in its proximity.

s-wave pairing As one can see in Fig. 6, the value of the s -wave order parameter does not vary significantly in the full range of values for V_M and ϕ . Thus, the amplitude reduction with respect to the bulk value is basically controlled by the presence of the half-metallic ferromagnet. Only by approaching the regime of $V_M \simeq V_0$ the effects of the spin active barrier become more relevant leading to a strong suppression of the pairing amplitude. In this case it is possible to distinguish two different behaviors corresponding to the spin-mixing or spin-flip barrier regime. Spin-mixing effects (i.e. $\phi = 0$) are not much relevant for the s -wave proximity effect as the pair amplitude exhibits only a slight reduction as one tunes the spin-dependent scattering from the regime $\rho = 0$ to $\rho \simeq 1$. This can be understood because the change of V_M tends to reinforce the magnetization even at the barrier site. There, the proximity between the half-metal ferromagnet and the superconductor leads to a matching of the magnetization from full- to zero-spin polarization in moving through the interface. Otherwise, spin-flip mechanisms lead to a larger reduction of the pair amplitude when approaching the limit $\rho \rightarrow 1$. In this case, the increase of the transverse magnetization (parallel to x in the spin space) at the barrier site leads to extra scattering for the singlet pairs that in turn sums up to the pair breaking effect due to the presence of the half-metal ferromagnet in a way to get about a 70% reduction.

Chiral p-wave pairing Consider next the case of chiral p -wave pairing (i.e. $\Delta \sim p_x + ip_y$) on the superconducting side of the junction. The chiral state exhibits time reversal symmetry breaking for a spin triplet configuration. It is well known that the interface properties can be quite unusual even

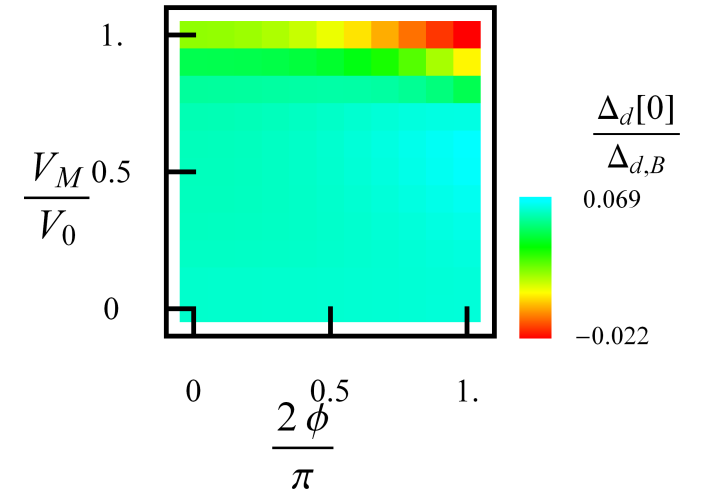


FIG. 9: (Color online) Color map the $d_{x^2-y^2}$ pairing amplitude at the interface $\Delta_d[0]$ with respect to the bulk value $\Delta_{d,B}$ as a function of the scaled misalignment angle $2\phi/\pi$ and the ratio of the magnetic barrier strength with respect to the non-magnetic one, V_M/V_0 . The non magnetic scattering potential has an amplitude $V_0 = 2t$.

at the boundary with the vacuum due the possibility of emergent exotic edge states. Here, we analyze the consequences of spin-mixing and spin-flip barrier processes on the two p -wave components separately. Though the gap amplitude is isotropic in k -space, as for the s -wave symmetry, the pairing amplitudes along x and y evaluated at the interface exhibit a completely different behavior. There are many distinguishing features that can be extracted from inspecting Figs. 7 and 8. Regarding effects induced by spin-mixing and spin-flip processes, note that i) spin-mixing and spin-flip reduce the pair breaking effects due to the proximity with the half-metal, ii) the reduction is not equivalent for the x and y components, iii) the pair breaking effects are more pronounced for the p_x than the p_y component. Indeed, for the case i) one notices in Figs. 7 and 8 that in the regime $V_M/V_0 \sim 1$, the pair amplitude tends to grow at any given angle with a slope that is more pronounced for the p_x component as compared to the p_y one. Concerning the point ii), the maximum of the pairing amplitude occurs at the phase diagram positions individuated by $(\phi, V_M/V_0) = (0, 1)$ and $(\phi, V_M/V_0) = (\pi/2, 1)$ for the p_x and the p_y amplitude, respectively. We argue that the presence of Andreev bound states in the spectrum, due to the change of sign of the p_x component in the direction perpendicular to the interface, leads to a more significant barrier influence of the correspondent pairing component with respect to the p_y one.

d-wave pairing In Fig. 9, we show the evolution of the interface d -wave pairing amplitude in terms of the scaled angle and scattering barrier parameters. Recall that for the chosen junction geometry there are no Andreev bound states in proximity to the half-metal. Hence, even though the pairing is anisotropic, the absence of Andreev states leads us to expect a behavior similar to the s -wave case. Indeed, the profile of the d -wave pairing amplitude at the interface is similar to that of the isotropic s -wave with an increase of the pair breaking effects in the regime of large spin-mixing and spin-flip. However, it is worth pointing out that close to the regime of

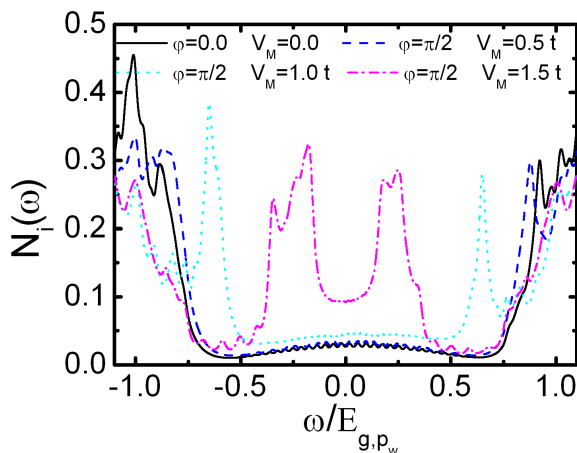


FIG. 10: (Color online) Density of states for the chiral p -wave evaluated at one representative site position ($i = 2$) within the range of one superconducting coherence length from the barrier ($i = 0$). The non magnetic potential has a value of $V_0 = 0.5t$.

maximal spin-flip scattering ($\phi = \pi/2$), where the orientation of the magnetic moment at the interface is perpendicular to the easy axis of pair formation, the combination of the spin-flip and the presence of the half-metal leads to a global phase change in the d -wave amplitude. This is reminiscent of the oscillating behaviour one would expect in a conventional ferromagnet/superconductor junction. Here, it is the anisotropy of the pairing that favors the formation of small oscillations in proximity of the barrier.

Interface density of states (DOS) In the previous section, we saw how a finite subgap conductance was obtained even in the strong tunnelling limit when the superconducting pairing was unconventional and the interface allowed for spin-flip processes. We speculated that the physical explanation behind this phenomenon was the generation of surface bound-states, appearing due to an interplay between the spin-active properties of the interface and the internal phase of the superconducting order parameter. In the absence of a spin-active interface, we found that subgap tunnelling vanished completely. We now investigate whether such surface bound-states are truly present or not within the lattice BdG-model, by focusing on the p -wave chiral type of pairing. This is expected to yield Andreev bound states for the geometry given in Fig.5.

In Fig.10, we show the behavior of the total DOS

$$N_i(\omega) = N_{i\uparrow}(\omega) + N_{i\downarrow}(\omega)$$

evaluated at one representative site position within a range of one superconducting coherence length from the barrier. There is a substantial difference in the results for the total DOS obtained when comparing the case of a complete non-magnetic barrier ($\phi = 0$ and $V_M = 0$) with the case of a pure spin-flip barrier scattering potential ($\phi = \pi/2$ and a varying V_M). The energy has been rescaled with respect to the gap amplitude E_{g,p_w} determined inside the superconductor within the same formalism, that is at a position where the DOS exhibits a full gap as expected for the chiral p -wave symmetry and the order parameter is uniform and unaffected by the interfaces. Note that for non-zero ϕ the change in the amplitude of V_M leads to extra midgap edge states. The energy of these states depend strongly on the magnetic barrier potential. Indeed, they appear at the edge of the gap for small values of V_M and as the amplitude of the magnetic moment at the barrier increases by tuning V_M , they shift towards low energies. The asymmetry of the resonant spectra is related to the presence of a small, but finite spin polarization proximate to the barrier on the superconducting side.

V. SUMMARY

In summary, by means of continuum and lattice BdG formalisms we have computed the conductance spectra, superconducting order parameter, and the density of states of a bilayer system made of a half-metal and an unconventional superconductor which are brought into contact through a spin active tunneling. These quantities have been computed for different forms of the pairing amplitude both for spin singlet s - and d -wave as well as spin triplet chiral p -wave symmetry. We

have shown how the spin-flip and spin-mixing scattering processes at the interface influence the structure of the superconducting order parameter in the case of different pairing symmetries, namely s -wave, chiral p -wave, and d -wave pairing. These scattering processes lead to different charge transport features such as subgap conductance and midgap Andreev assisted tunnelling due to resonant states, depending on which pairing symmetries are considered. The novel subgap features we find are present only for a non-zero misalignment between the half-metallic magnetization and the magnetic moment of the barrier. The energy position of the Andreev assisted charge processes turns out to be sensitive to changes in the ratio between the magnetic and non-magnetic scattering potential at the interface. We have also studied the pairing amplitude in a lattice model and computed its dependence at the interface on the barrier scattering strength, as well as its dependence on the misalignment angle between the half-metal magnetization and the barrier spin moment. For the case of a spin triplet chiral p -wave, midgap states at non zero misalignment angle between the half-metal magnetization the barrier spin moment have been found by computing the density of

states of the superconductor close to the interface. A hallmark of such edge states is the strong dependence of the ratio between the magnetic and non-magnetic scattering potential in the subgap DOS. Finally, we point out that the present study reveals highly non-trivial features of the proximity effect between a half-metal and an unconventional superconductor in the presence of a spin active interface even without invoking the occurrence of exotic mixed parity pair components. The present analysis is the starting point for further investigation of the role played by induced or subdominant pairing amplitudes in heterostructures based on half-metal and unconventional superconductors.

Acknowledgments

T. Yokoyama is acknowledged for useful discussions. J.L. and A.S. were supported by the Norwegian Research Council Grant No. 167498/V30 (STORFORSK).

-
- ¹ F. S. Bergeret *et al.*, Rev. Mod. Phys. **77**, 1321 (2005).
 - ² A. I. Buzdin, Rev. Mod. Phys. **77**, 935 (2005).
 - ³ J. Bardeen, L. N. Cooper, and J. R. Schrieffer, Phys. Rev. **108**, 1175 (1957); J. Bardeen, L. N. Cooper, and J. R. Schrieffer, Phys. Rev. **106**, 162 (1957).
 - ⁴ V. L. Berezinskii, Pisma Zh. Eksp. Teor. Fiz. **20**, 628 (1974).
 - ⁵ M. Eschrig, T. Löfwander, Th. Champel, J. C. Cuevas and G. Schön, J. Low Temp. Phys. **147** 457 (2007).
 - ⁶ Y. Tanaka *et al.*, Phys. Rev. Lett. **99**, 037005 (2007)
 - ⁷ F. S. Bergeret, A. F. Volkov, and K. B. Efetov, Phys. Rev. Lett. **86**, 4096 (2001).
 - ⁸ V. V. Ryazanov, V. A. Oboznov, A. Yu. Rusanov, A. V. Veretennikov, A. A. Golubov, and J. Aarts, Phys. Rev. Lett. **86**, 2427 (2001).
 - ⁹ A. F. Volkov, F. S. Bergeret, and K. B. Efetov, Phys. Rev. Lett. **90**, 117006 (2003)
 - ¹⁰ F. S. Bergeret, A. F. Volkov, and K. B. Efetov, Phys. Rev. B **68**, 064513 (2003)
 - ¹¹ M. Eschrig, J. Kopu, J. C. Cuevas, and G. Schön, Phys. Rev. Lett. **90**, 137003 (2003)
 - ¹² V. Braude and Yu. V. Nazarov, Phys. Rev. Lett. **98**, 077003 (2007).
 - ¹³ Y. Asano, Y. Tanaka, and A. A. Golubov, Phys. Rev. Lett. **98**, 107002 (2007); Y. Asano, Y. Sawa, Y. Tanaka, and A. A. Golubov, Phys. Rev. B **76**, 224525 (2007)
 - ¹⁴ R. S. Keizer, S. T. B. Goennenwein, T. M. Klapwijk, G. Miao, G. Xiao, and A. Gupta, Nature (London) **439**, 825 (2006).
 - ¹⁵ Ya. V. Fominov, A. F. Volkov, and K. B. Efetov, Phys. Rev. B **75**, 104509 (2007)
 - ¹⁶ T. Yokoyama, Y. Tanaka, and A. A. Golubov, Phys. Rev. B **75**, 134510 (2007)
 - ¹⁷ Y. Asano, Y. Tanaka, A. A. Golubov, and S. Kashiwaya, Phys. Rev. Lett. **99**, 067005 (2007)
 - ¹⁸ K. Halterman, P. H. Barsic, and O. T. Valls, Phys. Rev. Lett. **99**, 127002 (2007)
 - ¹⁹ Y. Tanaka and A. A. Golubov, Phys. Rev. Lett. **98**, 037003 (2007).
 - ²⁰ M. Eschrig, T. Lofwander, T. Champel, J. C. Cuevas, J. Kopu, G. Schön, J. Low Temp. Phys. **147**, 457 (2007).
 - ²¹ J. Linder, T. Yokoyama, and A. Sudbø, Phys. Rev. B **77**, 174507 (2008); J. Linder, T. Yokoyama, Y. Tanaka, Y. Asano, and A. Sudbø, Phys. Rev. B **77**, 174505 (2008).
 - ²² M. Eschrig and T. Löfwander, Nature Phys. **4**, 138 (2008).
 - ²³ K. Halterman, O. T. Valls, and P. H. Barsic, Phys. Rev. B **77**, 174511 (2008).
 - ²⁴ J. Linder and A. Sudbø, Phys. Rev. B **75**, 134509 (2007); J. Linder, T. Yokoyama, and A. Sudbø, Phys. Rev. B **77**, 174514 (2008)
 - ²⁵ L. N. Bulaevskii, V. V. Kuzii, and A. A. Sobyenin, Pis'ma Zh. Eksp. Teor. Fiz. **25**, 314 (1977) [JETP Lett. **25**, 290 (1977)].
 - ²⁶ A. I. Buzdin, L. N. Bulaevskii and S. V. Panyukov, Pis'ma Zh. Eksp. Teor. Fiz. **35**, 147 (1982).
 - ²⁷ E. Koshina and V. Krivoruchko, Phys. Rev. B **63**, 224515 (2001)
 - ²⁸ T. Kontos, M. Aprili, J. Lesueur, F. Gent, B. Stephanidis, and R. Boursier, Phys. Rev. Lett. **89**, 137007 (2002)
 - ²⁹ A. Buzdin and A. E. Koshelev, Phys. Rev. B **67**, 220504 (2003)
 - ³⁰ M. Houzet, V. Vinokur, and F. Pistolesi, Phys. Rev. B **72**, 220506 (2005)
 - ³¹ A. Cottet and W. Belzig, Phys. Rev. B **72**, 180503 (2005)
 - ³² J. W. Robinson, S. Piano, G. Burnell, C. Bell, and M. G. Blamire, Phys. Rev. Lett. **97**, 177003 (2006)
 - ³³ G. Mohammadkhani and M. Zareyan, Phys. Rev. B **73**, 134503 (2006)
 - ³⁴ J. Linder, T. Yokoyama, D. Huertas-Hernando, and Asle Sudbø, Phys. Rev. Lett. **100**, 187004 (2008)
 - ³⁵ M. Cuoco, W. Saldarriaga, A. Polcari, A. Guarino, O. Moran, E. Baca, A. Vecchione, and P. Romano, Phys. Rev. B **79**, 014523 (2009); G. Annunziata, M. Cuoco, C. Noce, A. Romano, and P. Gentile, Phys. Rev. B **80**, 012503 (2009).
 - ³⁶ T. Champel, M. Eschrig, Phys. Rev. B **71**, 220506(R) (2005); T. Champel, M. Eschrig, Phys. Rev. B **72**, 054523 (2005); T. Champel, T. Löfwander, and M. Eschrig, Phys. Rev. Lett. **100**, 077003 (2008)
 - ³⁷ A. F. Volkov and K. B. Efetov, Phys. Rev. B **78**, 024519 (2008)
 - ³⁸ J. Kopu, M. Eschrig, J. C. Cuevas, and M. Fogelström, Phys. Rev. B **69**, 094501 (2004)
 - ³⁹ J. Linder, T. Yokoyama, A. Sudbø, M. Eschrig, Phys. Rev. Lett.

- 102**, 107008 (2009)
- ⁴⁰ C.-R. Hu, Phys. Rev. Lett. **72**, 1526 (1994)
- ⁴¹ Y. Tanaka and S. Kashiwaya, Phys. Rev. Lett. **74**, 3451 (1995)
- ⁴² M. Cuoco, A. Romano, C. Noce, and P. Gentile, Phys. Rev. B **78**, 054503 (2008); A. Romano, M. Cuoco, C. Noce, P. Gentile, and G. Annunziata, Phys. Rev. B **81**, 064513 (2010).
- ⁴³ V. N. Krivoruchko and V. Yu. Tarenkov, Phys. Rev. B **78**, 054522 (2008)
- ⁴⁴ L. R. Tagirov, Physica C **307**, 145 (1998); L. R. Tagirov, Phys. Rev. Lett. **83**, 2058 (1999).
- ⁴⁵ A. Yu. Rusanov, S. Habraken, and J. Aarts, Phys. Rev. B **73**, 060505(R) (2006).
- ⁴⁶ I. C. Moraru, W. P. Pratt, Jr., and N. O. Birge, Phys. Rev. Lett. **96**, 037004 (2006).
- ⁴⁷ I. C. Moraru, W. P. Pratt, Jr., and N. O. Birge, Phys. Rev. B **74**, 220507(R) (2006).
- ⁴⁸ I. Baladie and A. Buzdin, Phys. Rev. B **64**, 224514 (2001).
- ⁴⁹ Ya. V. Fominov, N. M. Chtchelkatchev, and A. A. Golubov, Phys. Rev. B **66**, 014507 (2002).
- ⁵⁰ T. Löfwander, T. Champel, and M. Eschrig, Phys. Rev. B **75**, 014512 (2007).
- ⁵¹ P. Cadden-Zimansky, Ya. B. Bazaliy, L. M. Litvak, J. S. Jiang, J. Pearson, J. Y. Gu, Chun-Yeol You, M. R. Beasley, and S. D. Bader, Phys. Rev. B **77**, 184501 (2008).
- ⁵² S. Kashiwaya, Y. Tanaka, N. Yoshida, and M. Beasley, Phys. Rev. B **60**, 3572 (1999)
- ⁵³ Y. Asano, Y. Tanaka, and S. Kashiwaya, Phys. Rev. B **69**, 134501 (2004).